

Fermi–LAT Observations toward the Galactic Center

Simona Murgia

Department of Physics and Astronomy
University of California, Irvine, CA 92697, USA
email: smurgia@uci.edu

Abstract. The inner region of the Milky Way is one of the most interesting and complex regions of the γ -ray sky. Intense interstellar emission and point sources contribute to it, as well as other potential components such as an unresolved population of point sources and dark matter. In recent years, claims have been made of an excess consistent with a dark matter annihilation signal in the data collected with the *Fermi* Large Area Telescope (*Fermi*–LAT). Although these results are intriguing, the complexity involved in modeling the foreground and background emission from conventional astrophysical sources of γ -rays makes a conclusive interpretation of these results challenging. In these proceedings, I discuss *Fermi*–LAT observations of the Galactic center region, the methodology for point source detection and treatment of the interstellar emission, the characterization of the GeV excess, and implications for dark matter.

Keywords. Keyword1, keyword2, keyword3, etc.

1. Introduction

The region surrounding the Galactic center (GC) is among the brightest and most complex in high-energy γ -rays, with on-going massive star formation providing all types of known or suspected cosmic ray (CR) and γ -ray sources. The region is also predicted to be the brightest source of γ -rays associated with annihilation or decay of dark matter (DM). The γ -ray emission in the Galaxy is predominantly due to the interactions of CR particles with the interstellar gas and radiation fields. This interstellar emission (IE) is a fore-/background against which γ -ray point sources are detected. An excess in the *Fermi*–LAT data in the direction of the GC was first claimed in Goodenough *et al.* (2009). More recent analyses confirm the presence of the excess (e.g. Hooper *et al.* (2011), Hooper *et al.* (2011), Abazajian *et al.* (2012), Hooper *et al.* (2013), Gordon *et al.* (2013), Abazajian *et al.* (2014), Daylan *et al.* (2014), Calore *et al.* (2015)). The excess is claimed to be spatially consistent with DM annihilation for an Navarro, Frenk, and White (NFW, Navarro *et al.* (1996)) density distribution with slope $\gamma = 1.1 - 1.3$ centered at the location of the GC supermassive black hole, Sgr A*. Deviations from a spherically symmetric morphology are disfavored and the excess extends to at least 10° from the Galactic plane. The spectrum is consistent with a WIMP mass of ~ 50 (~ 10) GeV/ c^2 if annihilating predominantly into hadronic (leptonic) final states, with an annihilation cross-section compatible with a thermal relic. Alternative interpretations for this excess have been proposed. Notably, a population of unresolved pulsars is found plausible and compatible with the observed excess (see e.g. Abazajian *et al.* (2014), O’Leary *et al.* (2015), Brandt *et al.* (2015)). More recently, this hypothesis has been tested with non-poissonian photon statistics template analysis (Lee *et al.* (2015), Lee *et al.* (2016)) and with wavelet decomposition (Bartels *et al.* (2016)). These are promising ways to disentangle an extended component in the data that is more likely to originate from a population of discrete γ -ray emitters rather than with the continuous emission predicted for DM

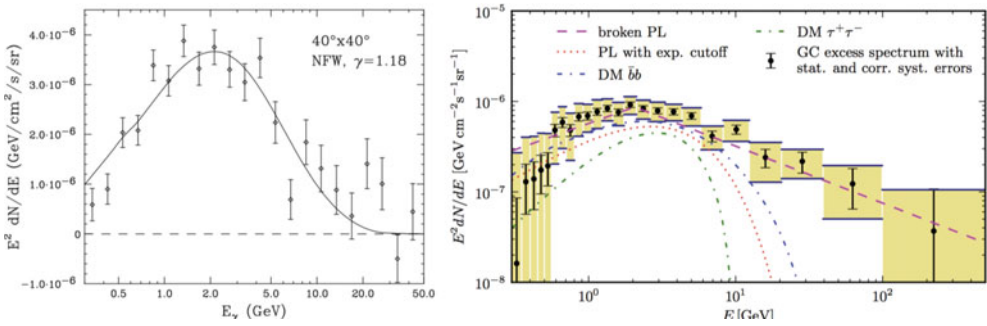


Figure 1. Spectrum of the GC excess from Daylan *et al.* (2014) (*left*), and Calore *et al.* (2015) (*right*).

annihilation (although DM substructures would contribute to the discrete emission.) Finally, cosmic ray (CR) proton or electron outbursts interpretations (e.g. Carlson *et al.* (2014), Petrovic *et al.* (2014), Cholis *et al.* (2015)) have also been proposed, although they arguably require a larger degree of fine tuning to explain all aspects of the excess.

2. Modeling of the Galactic Interstellar Emission and Results

The Galactic IE is generated by CR particles interacting with the interstellar gas and radiation field. The physical processes that contribute to this emission are: π^0 -decay, i.e. inelastic scattering of CR nuclei with the interstellar gas producing π^0 's and, in turn, γ -rays from their decay; bremsstrahlung by electrons and positrons on the interstellar gas; Inverse Compton (IC) scattering, i.e. CR electrons and positrons up-scattering the photons in the interstellar radiation field (ISRF) of the Galaxy to γ -ray energies. Modeling this emission requires knowledge of the origin and propagation of CRs, which is particularly uncertain for the GC region, where CR intensities, density of the ISRF and gas are highest and most uncertain and where there is a significant fore-/background contribution with long integration path over the entire Galactic disc. In addition, the many energetic sources near to or in the line of sight of the GC are difficult to disentangle from the IE. Two approaches have been most often employed to model the γ -ray IE towards the GC. One is to adopt the IE models (IEMs) provided by the *Fermi*-LAT Collaboration[†]. These are designed to flatten residuals over extended regions of the sky, for the study of point sources and sources with small extension in the *Fermi*-LAT data. These models often include patches to absorb positive residuals and since some of the patches are in and about the GC, the interpretation of additional extended excesses in this region is uncertain. The other approach is to use the CR propagation code GALPROP[‡], which provides physically motivated models for the IE, but does not fully capture the complexity of the Galaxy. Fig. 1 illustrates the difference in the spectrum of the GC excess when the *Fermi*-LAT Collaboration models for point source analysis (left panel, Daylan *et al.* (2014)), or GALPROP (right panel, Calore *et al.* (2015)) are employed. In both cases the spectrum of the GC excess peaks at a few GeV, however there is a strong dependence on the IEM at higher energies. Both of these analyses use established γ -ray source catalogs to model point sources.

An alternative and novel approach to determine the IEM and point sources in the inner Galaxy has been employed by the *Fermi*-LAT Collaboration (Ajello *et al.* (2016)).

[†] <http://fermi.gsfc.nasa.gov/ssc/data/access/lat/BackgroundModels.html>

[‡] <http://galprop.stanford.edu>

Specialized IEMs are constructed for a $15^\circ \times 15^\circ$ region about the direction of the GC to separate the emission from the inner ~ 1 kpc of the GC from the rest of the Galaxy in the 1–100 GeV energy range. A catalog of point sources for the $15^\circ \times 15^\circ$ region is self-consistently constructed using these IEMs. A major uncertainty affecting predictions of the IE toward the inner Galaxy is the spatial distribution of CR sources. In this analysis, the Yusifov *et al.* (2004) pulsar distribution (“Pulsars”) and the distribution of OB-stars (“OB stars”, Bronfman *et al.* (2000)) are used as proxies for the CR source distribution as they cover a broad range in its radial extent. Two IEMs from Ackerman *et al.* (2010), corresponding to these two assumptions for the CR source distribution, are employed as the baseline IEMs for this analysis, and are tuned to the *Fermi*–LAT data (excluding the $15^\circ \times 15^\circ$ region about the GC) for improved fore-/background determination. The γ -ray intensity maps, calculated by GALPROP in Galactocentric annuli, are used as templates for the IEM tuning procedure together with an isotropic component and a model for γ -ray emission associated with Loop I (Wolleben *et al.* (2007)). The procedure generates four IEMs, labeled: “Pulsars, intensity-scaled”, “Pulsars, index-scaled”, “OB stars, intensity-scaled”, “OB stars, index-scaled”. The IEMs differ in the assumed distribution of the sources of CRs (Pulsars or OB stars), and in the procedure employed to scale the γ -ray intensity of the fore-/background components outside of the $15^\circ \times 15^\circ$ region to the data: the intensity only for the “intensity-scaled” models, or the intensity and additional degrees of freedom in the spectrum of the gas-related IE interior to the solar circle for the “index-scaled” models. The normalization parameters for the templates are determined in a series of fits to the data, starting at high latitudes for the local components and then working from the outer Galaxy to the inner Galaxy, always fixing the already determined normalization parameters in subsequent fits. After this scaling, the agreement between data and model has improved for all baseline models and scaling procedure. It is not straightforward to identify a best IEM and consequently, all four (Pulsars/OB stars, intensity-/index-scaled) IEMs are used to estimate the fore-/background toward the $15^\circ \times 15^\circ$ region about the GC.

A list of point sources is determined for the $15^\circ \times 15^\circ$ region, concurrently with the IE. The wavelet based algorithm PGWave (Damiani *et al.* (1997)), which makes minimal assumption on the background, is employed to initially extract the position of point source candidates in the $15^\circ \times 15^\circ$ region, while their spectral properties and refinements on their position are determined by a maximum likelihood fit for each of the fore-/background models and concurrently with the IE in the $15^\circ \times 15^\circ$ region. The intensities for the IE from the innermost 1 kpc are determined by fitting the data in this region concurrently with the point source candidates, while the fore-/background models are held constant. This procedure is repeated until no significant point-like excesses remain in the residuals. Figures 2 and 3 show the differential flux and residuals for the Pulsars IEMs (the OB stars IEMs display very similar trends.)

The fore-/background is found to account for most of the emission in the region for all four IEMs. The fitted IC for the inner 1 kpc is bright, more than predicted by the baseline models (6-30x), which might imply more intense ISRF and/or CR electron density over the inner region. The gas π^0 intensities however are subdominant and much dimmer than in the baseline models. For the intensity-scaled variant of the IEMs, the data-model agreement is within 5-10% over the $15^\circ \times 15^\circ$ region up to 10 GeV. The models are too bright below 2 GeV and this disagreement is correlated with the Galactic plane, which might be pointing to an issue with the modeling of the spectra of the CR nuclei. The agreement is generally better for the index-scaled models. Above ~ 10 GeV, the intensity-scaled models increasingly underpredict the data, while the index-scaled models overpredict the data. At a few GeV all models underpredict the data and the excess

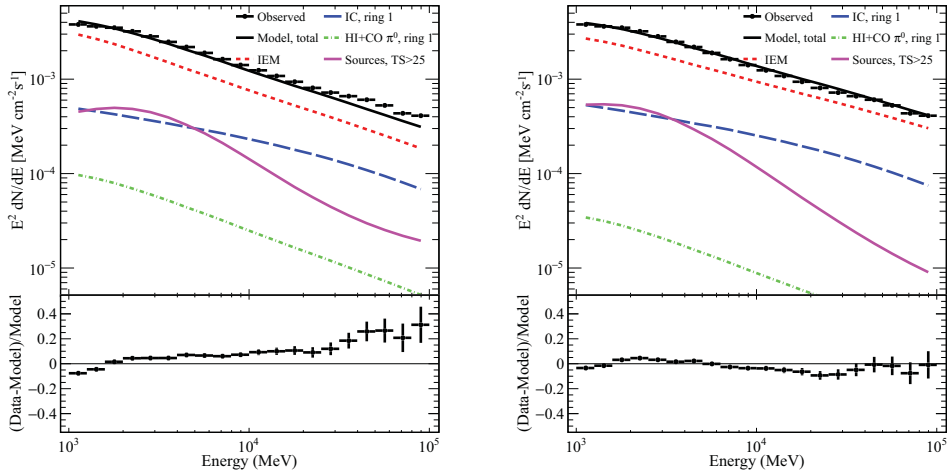


Figure 2. Differential fluxes for the $15^\circ \times 15^\circ$ region about the GC for the Pulsars intensity- (*left*) and index-scaled (*right*) IEMs. Line styles: solid (total model), long-dash (IC, annulus 1), dot-dash (H I and CO gas π^0 -decay, annulus 1), dot-dot-dot-dash (point sources), dash (Galactic IE excluding annulus 1 for IC, H I and CO gas π^0 -decay). Solid circles: data.

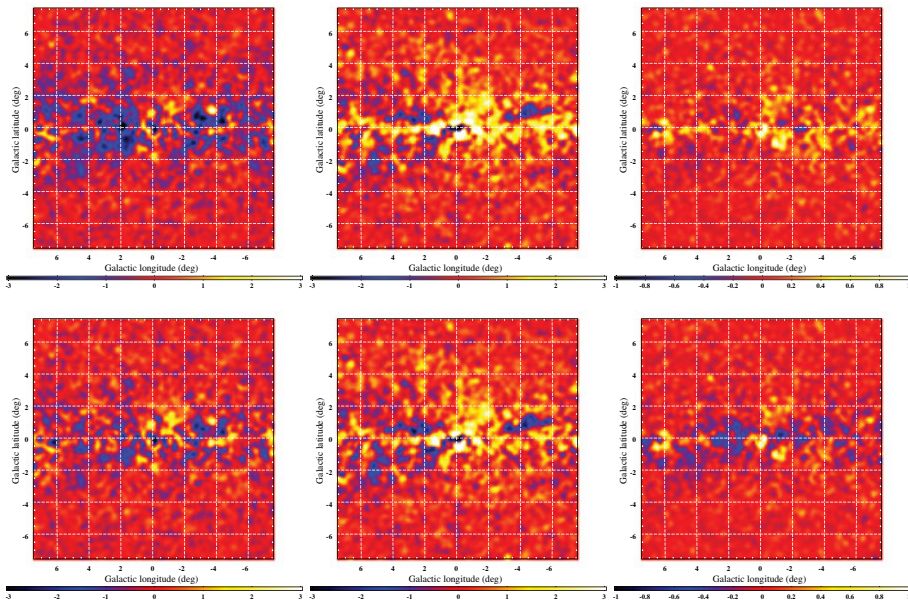


Figure 3. Residual counts for the $15^\circ \times 15^\circ$ region about the GC for the Pulsars IEMs for energy ranges 1 – 1.6 GeV (*left*), 1.6 – 10 GeV (*middle*), and > 10 GeV (*right*) for the intensity- (*top*) and index-scaled (*bottom*) variants. The color scale is in counts/0.1 deg^2 pixel.

appears to be extended and distributed around the GC, which might indicate the presence of a new extended component in the data.

This possibility is explored by including templates that are peaked at the GC: a set of two-dimensional Gaussians with varying widths; DM annihilation or decay templates (a NFW profile is assumed); gas-like morphologies are also considered. The spectrum is modeled with a power law function with an exponential cutoff (this has some flexibility to model a pulsar or a DM annihilation spectrum without supposing specific scenarios.)

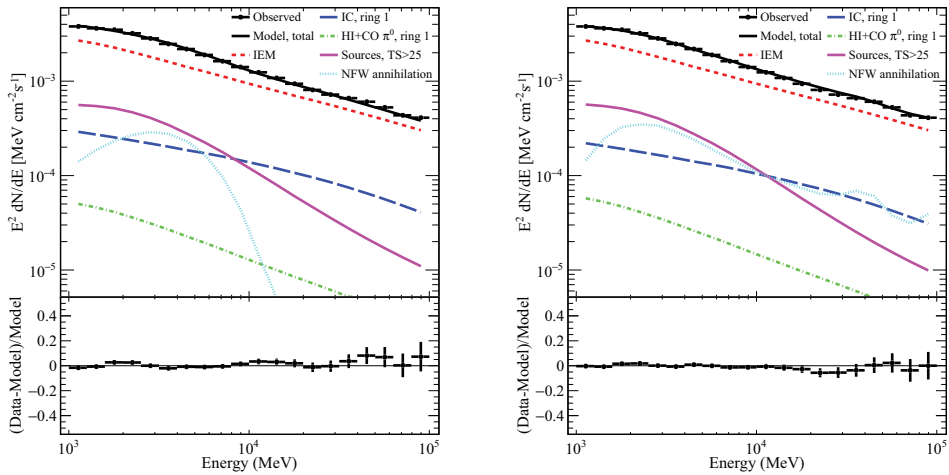


Figure 4. Differential fluxes for the $15^\circ \times 15^\circ$ region about the GC for the Pulsars index-scaled IEM including a DM annihilation template with spectrum modeled with a power law function with exponential cut-off (*left*) or power-law functions in 10 energy bins (*right*). Line styles: dot (DM annihilation); other lines as in Fig.2.

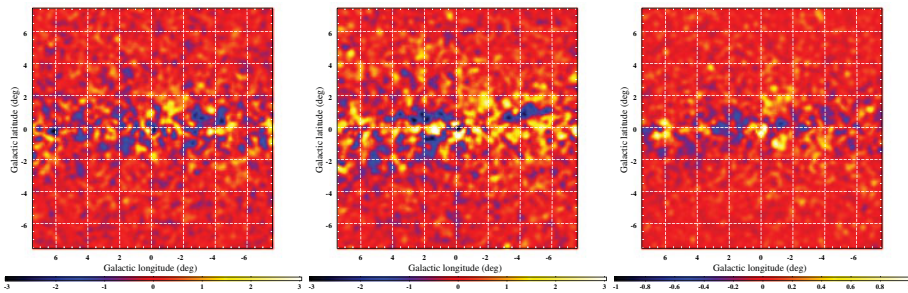


Figure 5. Residual counts for the $15^\circ \times 15^\circ$ region about the GC for the Pulsars index-scaled IEM together with the DM annihilation template for energy ranges 1 – 1.6 GeV (*left*), 1.6 – 10 GeV (*middle*), and > 10 GeV (*right*). The color scale is in counts/0.1 deg² pixel.

For each of the spatial templates listed above and for each of the IEMs, a maximum-likelihood fit is performed in the $15^\circ \times 15^\circ$ region. Among all the templates that have been tested, the DM annihilation template yields the most significant improvements in the data-model agreement for all IEMs. Figures 4 and 5 show the differential flux and residuals for the Pulsars index-scaled IEM, which yields the best agreement over the full energy range. The DM component spectrum depends strongly on the IEM, as shown in Fig. 6 for a power law function with exponential cut-off or power-law functions in 10 energy bins. Note that the the contribution to the GC excess spectrum above ~ 10 GeV is strongly reduced for the index-scaled IEMs (for the Pulsars, index-scaled, IEM the π^0 spectrum is consistently harder than the baseline across rings 2–4.) However, the spatial morphology at these energies might be DM-like (see also Linden *et al.* (2016), Horiuchi *et al.* (2016)).

The variation in the spectrum of the DM annihilation component is not easily ascribed to a covariance with only a single component of the model that is fitted over the $15^\circ \times 15^\circ$ region. For example, the ring 1 IC and H I-related π^0 -decay normalizations adjust in the fit to compensate for the additional template. The interplay between the centrally peaked positive residual template and the IE components is not surprising. Since the IC

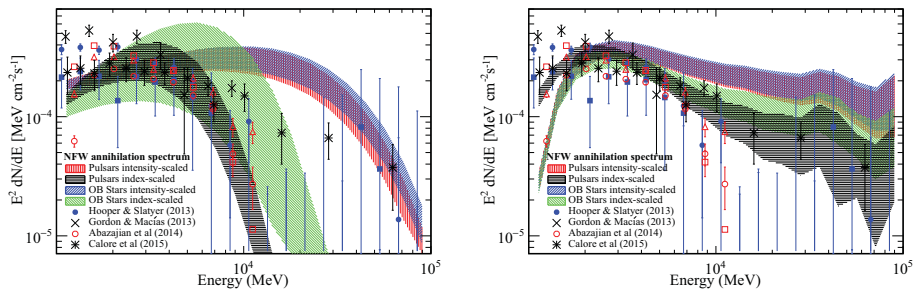


Figure 6. Differential fluxes in the $15^\circ \times 15^\circ$ region about the GC for the DM annihilation template with spectrum modeled with a power law function with exponential cut-off (*left*) or power-law functions in 10 energy bins (*right*). The envelopes include the fit uncertainties for the normalization and spectral index. Hatch styles: Pulsars, intensity-scaled (red, vertical); Pulsars, index-scaled (black, horizontal); OBstars, intensity-scaled (blue, diagonal-right); OBstars, index-scaled (green, diagonal-left). Results from selected other works are overlaid. *Filled symbols*: Hooper *et al.* (2013), different symbols bracket the results obtained when different regions of the sky are considered in the fit; *Angled crosses*: Gordon *et al.* (2013); *Open symbols*: Abazajian *et al.* (2014), front-converting events shown with triangles, front- and back-converting events shown with squares and circles, depending on the modelling of the fore-/background. *Stars*: Calore *et al.* (2015). Note: the overlaid results are rescaled to the DM content over the $15^\circ \times 15^\circ$ region for an NFW profile with index $\gamma=1$.

component is peaked toward the GC for all IEMs an additional template that is also peaked there will be attributed some flux when fit. However, the spectral parameters of the residual template are not solely determined by the fit with the IE components and point sources over the inner region about the GC; the fore-/background IE has an effect as well. This analysis yields 48 point sources in the $15^\circ \times 15^\circ$ with a test statistics (TS) > 25 (corresponding to a significance above $\sim 4\sigma$). These comprise the First *Fermi*-LAT Inner Galaxy Point Source Catalog (1FIG). Note that the sub-threshold point source candidates are also included in the maximum likelihood fit, along with those that satisfy the $TS > 25$ criterion for “detection” used for the 1FIG. Comparison with Greens SNR and ATNF (pulsar) catalogs have been performed, and three SNRs correspond to 1FIG sources that are new detections in high-energy γ -rays at *Fermi*-LAT energies. Compared to the Third *Fermi*-LAT Source Catalog (3FGL), 1FIG sources tend to be closer to the Galactic plane and many appear to trace features in the innermost gas templates and therefore might be mis-identified structured IE (see Fig. 7, left panel.) Understanding the interplay between point sources and IE in the region is important when determining unaccounted for point source contribution and interpretation of the GC excess.

The prescriptive method of determining the fore-/background IE, together with the self-consistent treatment of the point sources and IE for the inner ~ 1 kpc about the GC allows the least biased estimate to date to be made of the positive residual emission about the GC. Although a large formal statistical significance may be indicated for the detection of a DM component, fitting a centrally peaked profile does not account for all of the excess emission over the $15^\circ \times 15^\circ$ region. This can be seen in Fig. 5, where the residual emission does not appear distributed symmetrically about the GC below 10 GeV, and still has extended positive residuals even at higher energies along and about the plane. A more complete assessment of the uncertainties in the IEM (see Ajello *et al.* (2016) for a discussion) is required for a more robust characterization of the excess. Preliminary work addressing some of the limitations of the current IEMs is discussed in section 3.

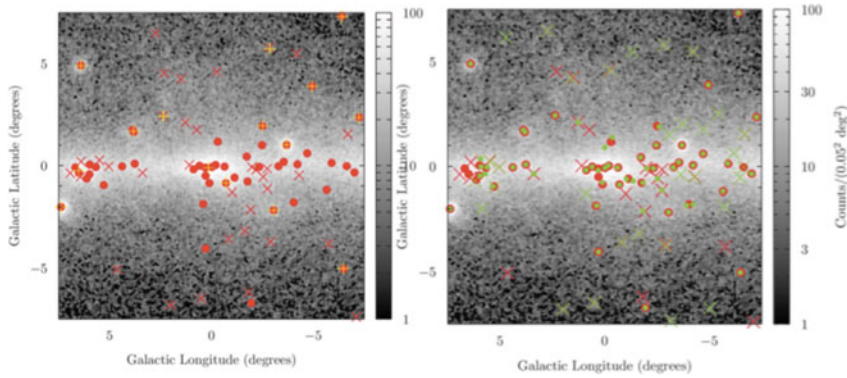


Figure 7. *Left:* 1FIG point sources overlaid to counts in the $15^\circ \times 15^\circ$ region. *Right:* 1FIG (red) overlaid to the point source list obtained by employing an IEM including 3D ISRF (green). Solid circles indicate point sources detected with $TS > 25$, while crosses correspond to sub-threshold sources.

3. 3D Interstellar Radiation Field

Limitations in the IEMs employed for the analysis of the *Fermi*-LAT GC data include the assumption of cylindrical symmetry. The density of CR sources and interstellar medium is associated with spiral arms, Galactic bar/bulge, and therefore is radially and azimuthally dependent. However, currently there are no detailed 3D models for the interstellar gas, radiation field, and cosmic-ray sources. Understanding these issues and addressing these limitations is crucial to confirm the presence and properties of additional components, dark matter or otherwise. Work is ongoing in addressing these limitations, e.g. improved gas maps (including 3D modeling, see Johannesson (2015)) and 3D modeling of the interstellar radiation field (ISRF) (see Porter (2016)). This will provide a considerable improvement in the characterization of the GC excess, if it persists, including a robust assessment of crucial features.

Initial work on the 3D modeling of the ISRF is underway. A more realistic model for the stellar luminosity has been implemented and tuned to multi-wavelength data (few μm and $\sim 100 \mu m$) (Porter (2016)). Based on this updated model of the ISRF, the predicted IC γ -ray intensity has been obtained and compared to its 2D ISRF counterpart. The fractional difference at ~ 1 GeV over all sky is shown in Fig. 8. The differences are more pronounced along the Galactic plane, and towards the GC, and indicate an asymmetry in the 3D ISRF IC which is not present in its 2D counterpart. To assess the impact of the revised ISRF on the analysis of the *Fermi*-LAT GC data, the *Fermi*-LAT Collaboration analysis described in the previous section has been repeated by employing the preliminary 3D ISRF with the Pulsars IEM, including the scaling of ring intensities for the determination of the fore-/background. The intensities for the innermost ring for H I and CO π^0 , IC emission, as well as point sources, are obtained by fitting the data in the $15^\circ \times 15^\circ$ region. The residual counts are shown in Fig. 9. Similar features as seen using the 2D ISRF models are present (see Fig. 3, top panels), but are enhanced. Interestingly, the excess towards the GC at 1.6 – 10 GeV appears brighter. Differential fluxes for the model, and individual model components, are shown in Fig. 10. IC ring 1 is still brighter compared to the baseline, similarly to the 2D ISRF case, but not as enhanced. In addition, the π^0 emission from the innermost gas ring is not as suppressed as in the 2D case compared to the baseline IEM. The point sources in the region also differ compared to the 2D ISRF. They are shown in Fig. 7 (right panel): 55 point sources with $TS > 25$ are found with the revised ISRF, compared to the 48 in the 1FIG. In summary,

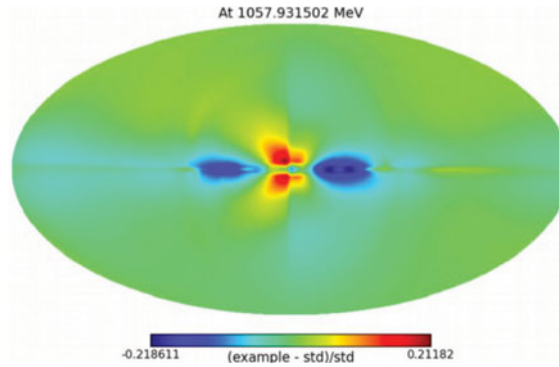


Figure 8. Fractional difference between IC γ -ray intensities for 3D (example) and 2D (std) ISRF.

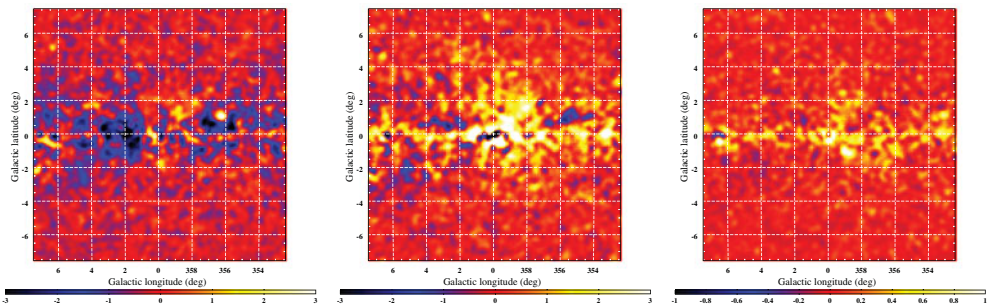


Figure 9. Residual counts for the $15^\circ \times 15^\circ$ region about the GC for the Pulsars, intensity-scaled, IEM with 3D ISRF for energy ranges 1 – 1.6 GeV (*left*), 1.6 – 10 GeV (*middle*), and > 10 GeV (*right*). The color scale is in counts/0.1 deg² pixel.

a revised IEM based on a more realistic 3D ISRF has been tested. It yields a IC template that is asymmetric with respect to the GC. This is an important consideration as a strong interplay is observed between the 2D ISRF IC ring 1 template with the DM template, both axisymmetric. The revised ISRF generates different results compared to 2D ISRF for the analysis of the inner Galaxy data at all stages of the analysis: scaling factors in fore-/background, inner 1 kpc components, and point sources. Work is in progress for improved determination of 3D ISRF, and inclusion of 3D distribution for CR electrons.

4. NFW Centroid

The centroid of the Milky Way DM halo is conventionally chosen to correspond to the location of Sgr A*, the dynamical center of the Milky Way. The possibility of an offset is explored by repeating the maximum likelihood fit for different locations of the centroid for the DM template (Karwin *et al.* (2016)). Its spectrum is modeled with a power law function with exponential cutoff, and a scan of the centroid position in a $1^\circ \times 1^\circ$ region centered at Sgr A*, in 0.2° intervals, is initially performed for all IEMs. At each grid point a maximum likelihood fit is performed. The grid size is extended as needed to enclose the minimum. The results are shown in Fig. 11 for each of the IEMs. The color scale shows the $2\Delta\log L$ as a function of Galactic latitude and longitude. The centroid position is offset from Sgr A* for all IEMs. The Pulsars, index-scaled model displays the largest offset, both in longitude (0.6°) and latitude (0.2°), while an offset in longitude is found

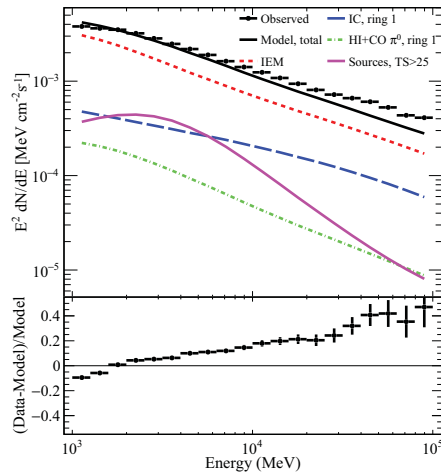


Figure 10. Differential fluxes for the $15^\circ \times 15^\circ$ region about the GC for the Pulsars intensity-scaled 3D ISRF IEM. Line styles as in Fig.4

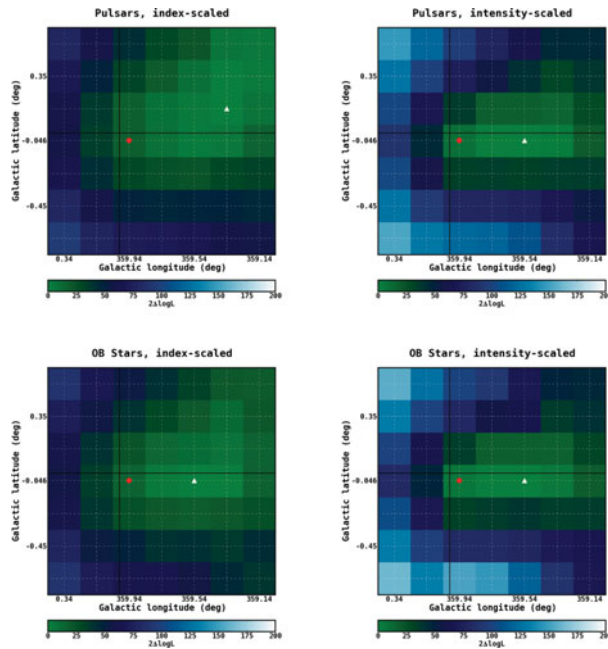


Figure 11. $2\Delta\log L$ scan in Galactic latitude and longitude of the position of the DM component centroid. The red circle is the position of Sgr A*, and the white triangle is the most likely position of the centroid.

for the other three IEMs (0.4°), within the grid accuracy. Sgr A* is therefore disfavored as the location of the NFW centroid at a 90% C.L. for this analysis. However, we cannot rule out that the offset is due to limitations on the IEMs. Deficits in the residual emission along the plane are more pronounced on the opposite side of the GC compared to the best fit position of the centroid and this asymmetry might be one of the causes of the observed offset. Improvements in modeling the IE are warranted to better determine the morphology of the excess.

5. Conclusions

The majority of γ -rays observed by *Fermi*-LAT in the inner Galaxy is likely due IE and point sources. An excess towards the GC is present in the data, and persists with best current estimates of IE and point sources. This is where a DM signal is predicted to be brightest, but alternative explanations cannot be excluded. The astrophysical background is currently a strong limitation in determining the origin of the excess, and further work to better model it is essential. This is crucial to confirm the presence and to determine the properties of this signal. In addition, other targets (e.g. dwarf spheroidal galaxies) and complementarity (direct detection and collider searches) will continue to test a DM interpretation of the GC excess.

References

- K. N. Abazajian & M. Kaplinghat, *Phys. Rev. D* **86**, 083511 (2012)
- K. N. Abazajian, N. Canac, S. Horiuchi & M. Kaplinghat, *Phys. Rev. D* **90**, no. 2, 023526 (2014)
- A. A. Abdo *et al.* [*Fermi*-LAT Collaboration], *Astropart. Phys.* **32**, 193 (2009)
- M. Ackermann *et al.* [*Fermi*-LAT Collaboration], *Phys. Rev. Lett.* **107**, 241302 (2011)
- M. Ackermann *et al.* [*Fermi*-LAT Collaboration], *Astrophys. J. Suppl.* **203**, 4 (2012)
- M. Ackermann *et al.* [*Fermi*-LAT Collaboration], *Phys. Rev. Lett.* **115**, no. 23, 231301 (2015)
- M. Ackermann *et al.* [*Fermi*-LAT Collaboration], *Astrophys. J.* **750** (2010) 1044
- M. Ajello *et al.* [*Fermi*-LAT Collaboration], *Astrophys. J.* **819** (2016) 1 44
- W. B. Atwood *et al.* [LAT Collaboration], *Astrophys. J.* **697**, 1071 (2009)
- R. Bartels, S. Krishnamurthy & C. Weniger, *Phys. Rev. Lett.* **116**, no. 5, 051102 (2016)
- T. D. Brandt & B. Kocsis, *Astrophys. J.* **812**, no. 1, 15 (2015)
- L. Bronfman, S. Casassus, J. May & L. A. Nyman, *Astron. Astrophys.* **358**, 521 (2000)
- F. Calore, I. Cholis & C. Weniger, *JCAP* **1503**, 038 (2015)
- E. Carlson & S. Profumo, *Phys. Rev. D* **90**, no. 2, 023015 (2014)
- I. Cholis, C. Evoli, F. Calore, T. Linden, C. Weniger & D. Hooper, *JCAP* **1512**, no. 12, 005 (2015)
- F. Damiani, A. Maggio, G. Micela, & S. Sciortino. *Astrophys. J.* **483** (1997) 350
- T. Daylan, D. P. Finkbeiner, D. Hooper, T. Linden, S. K. N. Portillo, N. L. Rodd & T. R. Slatyer, *Phys. Dark Univ.* **12**, 1 (2016)
- A. Geringer-Sameth & S. M. Koushiappas, *Phys. Rev. Lett.* **107**, 241303 (2011)
- L. Goodenough & D. Hooper, arXiv:0910.2998 [hep-ph].
- C. Gordon & O. Macias, *Phys. Rev. D* **88**, no. 8, 083521 (2013)
- D. Hooper & L. Goodenough, *Phys. Lett. B* **697**, 412 (2011)
- D. Hooper & T. Linden, *Phys. Rev. D* **84**, 123005 (2011)
- D. Hooper & T. R. Slatyer, *Phys. Dark Univ.* **2**, 118 (2013)
- S. Horiuchi, M. Kaplinghat & A. Kwa, arXiv:1604.01402 [astro-ph.HE].
- G. Johannesson, Talk at the Sixth International Fermi Symposium (2015)
- C. Karwin, S. Murgia, T. A. Porter, T. M. P. Tait, P. Tanedo, *In preparation.*
- S. K. Lee, M. Lisanti & B. R. Safdi, *JCAP* **1505**, no. 05, 056 (2015)
- S. K. Lee, M. Lisanti, B. R. Safdi, T. R. Slatyer & W. Xue, *Phys. Rev. Lett.* **116**, no. 5, 051103 (2016)
- T. Linden, N. L. Rodd, B. R. Safdi & T. R. Slatyer, arXiv:1604.01026 [astro-ph.HE].
- J. F. Navarro, C. S. Frenk & S. D. M. White, *Astrophys. J.* **462**, 563 (1996)
- R. M. O'Leary, M. D. Kistler, M. Kerr & J. Dexter, arXiv:1504.02477 [astro-ph.HE].
- J. Petrovic, P. D. Serpico & G. Zaharijas, *JCAP* **1410**, no. 10, 052 (2014)
- T. A. Porter, *In preparation.*
- M. Wolleben, *Astrophys. J.* **664**, 349 (2007)
- I. Yusifov & I. Kucuk, *Astron. Astrophys.* **422**, 545 (2004)